RSC Advances

ROYAL SOCIETY OF CHEMISTRY

www.rsc.org/advances

Enhanced electrical conductivity of Au-$LaNiO_3$ nanocomposite thin films by chemical solution deposition

H. L. Wang, X. K. Ning, Z. J. Wang†

Shenyang National Laboratory for Materials Science, Institute of Metal Research (IMR),

Chinese Academy of Sciences (CAS), 72 Wenhua Road, Shenyang 110016, China

Abstract

Au-$LaNiO_3$ (Au-LNO) nanocomposite films with 3.84 at% Au were firstly fabricated by one-step chemical solution deposition (CSD), and their electrical properties were investigated. Au nanoparticles with average size of approximately 10 nm were distributed uniformly in the LNO matrix. The nanocomposite films exhibit much lower room temperature resistivity (313 μΩ·cm) than the LNO films (1221 μΩ·cm). The role of Au nanoparticles in the composite films can be considered from two aspects: Firstly, the uniform distribution of Au nanoparticles provides a pathway with less scattering for the conduction of electrons. Secondly, Au nanoparticles can serve as nuclei seeds for the perovskite LNO phase to improve its crystalline quality. Transport property measurement reveals that the Au-LNO nanocomposite films exhibit a lower metal-insulator transition (MIT) temperature and suppression of weak localization due to the lower concentration of oxygen vacancy. The high-quality Au-LNO nanocomposite films with the excellent electrical conductivity are expected to be applicable as electrodes for ferroelectric and multiferroic films.

Keywords: Nanocomposite; Au-LNO thin film; transport property; chemical solution deposition

†Corresponding author; e-mail: wangzj@imr.ac.cn

Introduction

Among the family of the perovskite rare-earth nickelates, $LaNiO_3$ (LNO) is a strongly correlated metallic oxide, believed to be on the verge of a metal-insulator transition. [1,2] LNO has a rhombohedral crystal structure (a = 0.5461 nm, c = 0.6572 nm). In the pseudo-cubic form, LNO has a parameter of 0.384 nm matching well with most perovskite ferroelectric films that have been extensively studied for applications in microelectronics, micro-electromechanics, nonvolatile ferroelectric random-access memory devices, and energy harvesting devices.[3-6] The LNO thin films are extensively used as electrodes for ferroelectric and multiferroic films. However, the resistivity of the LNO thin films prepared on SiO_2/Si substrates is in a range of 750 ~ 2000 μΩ·cm, which is much higher than that of metal Pt films.[7,8] As a result, the high resistivity of LNO thin film as electrodes will inevitably cause degradation of ferroelectric properties. Therefore, from the viewpoint of application, it is of great importance to reduce the resistivity of polycrystalline LNO films on the SiO_2/Si substrates.

Recently, composite thin films of metal-perovskite oxides have produced a tremendous flurry of research interest because of their unique physical and chemical properties. For example, metal-dielectric nanocomposite films, such as Co-$BaTiO_3$, Au-$BaTiO_3$ and Ag-$PbTiO_3$ composite films, have showed enhanced optical and electrical properties.[9-11] Adding metal nanoparticles into the conductive oxide could also reduce the resistivity of the composite films, such as Ag-ITO and Pt-LNO nanocomposite films.[12,13] In the Pt-LNO films fabricated by radiofrequency (RF)

co-sputtering, Pt particles formed a interconnected net-like nanostructure in the films, which provided effective conducting paths to reduce the electrical resistivity.[13] However, there are few works to study the effect of noble metal nanoparticles on the perovskite matrix. In this work, we firstly report that Au-LNO nanocomposite thin films with an excellent electrical conductivity can be prepared by one-step chemical solution deposition, and the effects of Au nanoparticles on the crystallization, microstructure, electrical transport property of the Au-LNO films were investigated.

Experimental

The precursor solution for the Au-LNO thin films was prepared from lanthanum nitrate ($La(NO_3)_3 \cdot 6\ H_2O$), nickel acetate ($Ni(CH_3COO)_2 \cdot 4\ H_2O$) and gold chloride acid ($HAuCl_4 \cdot 3.5\ H_2O$). Acetic acid (CH_3COOH) and 2-methoxyethanol (2-MOE) were used as the solvent (mixed with a volume ratio of 1:3). Lanthanum nitrate, nickel acetate and gold chloride acid were dissolved in the mixed solvent at room temperature, respectively. Then three solutions were mixed together with constant stirring. Finally, clear and stable precursor solutions were obtained with LNO mole concentration 0.15 M and Au addition of 3.84 at%. After aging 24 hours, the solution was ready for spin-coating. Oxidized (100)-silicon wafers (1.0 μm of SiO_2) were used as the substrates. The LNO and Au-LNO films were coated onto SiO_2/Si substrates using a spin-coater operated at 4000 rpm for 60 s, respectively. The coated films were dried at 100 ℃ for 5 min on a hot plate, and then annealed at 600 ℃ for 30 min by using a conventional electric furnace in air atmosphere. The above steps were

repeated for several times to achieve the desired thickness.

Microstructure and crystallographic orientations of the Au-LNO films were characterized by θ-2θ scans of X-ray diffraction (XRD; Rigaku RINT2000, Cu Kα radiation) analysis. The microstructures of the films were characterized by transmission electron microscopy (TEM; Tecnai F20) and the TEM specimens were prepared by the standard procedure of cutting, gluing, slicing, grinding and finally ion milling. The chemical states of the elements in the films were determined by X-ray photoelectron spectroscopy (XPS, Thermo VG ESCALAB250,Al Kα 1486.6 eV). The room temperature resistivity was obtained by the standard four-probe method. Transport properties were measured by PPMS system (Quantum Design).

Results and discussions

The XRD patterns of the LNO and Au-LNO films grown on the SiO_2/Si substrates are shown in Fig. 1. The LNO films are crystallized into the perovskite phase and show a highly (100)-preferred orientation. Whereas, in the Au-LNO films, the peak intensity of the (001) and (002) planes of the LNO phase markedly decreases, while the (110) peak increases. Usually, forming of a preferred orientation in films is strongly dependent on the early stages of nucleation and growth. The above results suggest that the adding Au can affect nucleation and growth of the perovskite LNO in the crystallization process for the Au-LNO films. In addition, the diffraction peaks for (111) and (200) planes for the face centered cubic phase of Au can also be detected in the Au-LNO films, indicating that the Au-LNO films consist of two individual phases

of the LNO and Au. The full width at half maximum (FWHM) for the LNO (200) peak of the LNO films is about 0.55, while for the LNO (110) peak of the Au-LNO films is about 0.22, indicating that the Au-LNO films have higher crystalline quality than the LNO films. Moreover, compared with the XRD pattern of the LNO films, there is no shift for the LNO peaks in the Au-LNO film, implying that Au atoms or ions did not enter the LNO lattice. To clear this point, the chemical valence state of Au was also verified by XPS study.

The high-resolution Au 4*f* core level spectrum in the binding energy ranging from 80 eV to 92 eV is displayed in Fig. 2. One peak with the higher binding energy (87.7 eV) is identified as Au $4f_{5/2}$ core level line, and another one with the lower binding energy (84.0 eV) is identified as Au $4f_{7/2}$ core level line, which are consistent with the values reported for pure metal Au.[14] This result also indicates that Au as a single phase exists in the composite films.

The nanometer-scale distribution of the Au and LNO phase is characterized by TEM. Figure 3(a) shows a cross-sectional high-angle annular dark field (HAADF) image of the Au-LNO film. Au nanoparticles can be distinguished clearly from the LNO phase by Z-contrast, and one of them is noted by a red circle. The Au nanoparticles with a average grain size of about 10 nm uniformly distribute in the LNO matrix. In the Au-LNO nanocomposite films, because the Au content is low (only 3.84 at%), the Au nanoparticles can not connect with each other to form network conducting paths to reduce the electrical resistivity. This is different from the Pt-LNO nanocomposite films (36.1 at% of Pt) reported by Qiao and Bi.[13] Figure 3(b)

shows a HRTEM image of the Au-LNO film. The area with dark contrast exhibits a inter-planar spacing of 2.37 Å, corresponding to the Au (111) plane. According to XRD results, the d-spacing of the LNO (111) is determined to be 2.25 Å, and the lattice mismatch between the two (111) planes of Au and LNO is as small as about 5%. It can be seen that the LNO (111) planes is parallel to the Au (111) planes, implying that the Au nanoparticle served as nuclei seeds for the crystallization of its surrounding perovskite LNO phase. In fact, during crystallization process of the Au-LNO films, Au nanoparticles firstly crystallized before the LNO matrix due to that $HAuCl_4$ is readily decomposed to form Au nanoparticles when temperature rises to 200 °C.[15] According to the above experimental results, we can conclude that Au nanoparticles can serve as nuclei seeds for the crystallization of the perovskite LNO phase.

For the chemically stoichiometry of LNO, Ni is expected to be in a high valence state of Ni^{3+}. In fact, the Ni^{3+} state is thermodynamically unstable so that LNO has a strong tendency to exhibit mixed Ni^{3+} and Ni^{2+} due to the loss of oxygen during fabrication processes.[16] Figure 4 shows the O 1*s* core-level XPS spectra for the LNO and Au-LNO films. The major peak at the lower binding energy can be identified as lattice oxygen in LNO, which can be deconvoluted into Ni^{3+}-O (529.1 eV), La^{3+}-O (529.65 eV) and Ni^{2+}-O (530.3 eV) chemical bondings.[17] The smaller peak at the higher binding energy of 532 eV is associated with surface absorption oxygen resulting from the oxygen vacancies formed in perovskite oxides.[18] The concentration of oxygen vacancies in LNO can be quantitatively estimated by measuring the relative

peak area ratio of absorption oxygen/lattice oxygen. The ratio of absorption oxygen/lattice oxygen is 0.237 for the LNO films, while is 0.023 for the Au-LNO films. The lower concentration of oxygen vacancy in the Au-LNO films can be explained by the high crystalline quality of the Au-LNO films as indicated by the above XRD results. In addition, Au nanoparticles are well known for their remarkable catalytic behaviour.[19] In the crystallization process of the Au-LNO films, Au nanoparticles may promote the oxidation of $Ni^{2+} + 1/2\ O \rightarrow Ni^{3+} + 1/2\ O^{2-}$, which is benefit to stabilize Ni^{3+} state. As a result, the Au-LNO films show a better crystalline quality with lower concentration of oxygen vacancy compared with the LNO films. Previous study has revealed that among the defects formed during fabrication process, oxygen vacancies played a crucial role in affecting the electrical properties of LNO films.[20] It should be noted that the final annealing temperature can also affect the crystalline quality, oxygen content and Ni^{3+}/Ni^{2+} ratio of the matrix LNO. To control the oxygen concentration and Ni^{3+}/Ni^{2+} ratio in the Au-LNO nanocomposite films, future study on the effect of annealing temperature will be needed.

The electrical resistivity at room temperature for the Au-LNO and LNO films was measured using the standard four-point probe method. The resistivity for the Au-LNO films is 313 μΩ·cm, which is much lower than that of the LNO films (1221 μΩ·cm). To understand the dramatic decrease of the resistivity in the Au-LNO nanocomposite films, the micromechanism of resistivity is discussed. It is well known that $1/\rho = \sigma = en\mu_d$, where e is the electron charge, n is the electron density, μ_d is the electron drift mobility. The relation between the drift mobility μ_d and the mean

scattering time τ is given by $\mu_d = e\tau/m_{eff}$, where m_{eff} is the effective mass of electron. Therefore, the electrical resistivity of a material depends largely on the electron density n and effective mass of electron m_{eff}. For the LNO films in this study, the carrier density n is 1.7 x 10^{22} cm^{-3} calculated by Hall coefficient measurement, which is consistent with the value reported previously.[21] The effective mass m_{eff} of LNO is 11 m_e. The scattering frequency $1/\tau$ and the correlation length l are estimated to be 5.31 x 10^{14} s^{-1} and 1.57 Å, respectively. The Fermi velocity v_F is 8.35×10^6 cm/s. Since Au nanoparticles are immiscible in LNO phase, the value of electron density and Fermi velocity are estimated as $n \approx 1.91\times10^{22}$ cm^{-3} and $v_F \approx 1.42 \times 10^7$ cm/s for the Au-LNO films. The scattering frequency of electron in the Au-LNO films is approximately 2.51 x 10^{14} s^{-1}, nearly half of that in the LNO films. Therefore, we can conclude that although Au nanoparticles do not form the interconnected network conducting path, the uniformly distribution of Au nanoparticles can provide a path with less scattering for conduction of electrons. This may dramatically decrease the resistivity of the film. In addition, the effective mass of the Au-LNO composite films is estimated as $m_{eff} = lne^2\rho/v_F \approx 6.7\ m_e$. Compared with the value for strongly correlated LNO, the smaller m_{eff} for the Au-LNO composite indicates the broaden of the bandwidth which will further suppress weak localization to enhance the electrical property of the LNO matrix.

The temperature dependence of electrical resistivity for the LNO and Au-LNO films is shown in Fig. 5(a). The transport property can be discussed for two temperature ranges. At the high temperature region, both films demonstrate a metallic

behavior. We found that ρ(T) can be fitted well by the power law $\rho = \rho_0 + cT^{1.5}$, where ρ_0 is residual resistivity. According to Mathur's and Zhou's works, n = 1.5 means that strong correlations lead the system toward a quantum critical point in the vicinity of a magnetically ordered phase.[22,23] The weak ferromagnetism may originate from the coexistence of Ni^{3+} and Ni^{2+} due to the loss of oxygen as discussed above.[24,25] For the Au-LNO films, the value of ρ_0 is as low as 191 μΩ·cm, which is comparable with epitaxial LNO films on $SrTiO_3$ single-crystalline substrate.[26] As mentioned above, the crystalline quality of the perovskite LNO phase in the Au-LNO films is enhanced well by adding Au nanoparticles. At the low temperature range, both films showed a resistivity upturn which can be identified as metal-insulator transition (MIT). The MIT can be explained by the presence of quantum corrections to the conductivity (QCC).[26,27] The low-temperature dependence of the resistivity can be fitted by $\rho = 1/(\sigma_0 + alnT) + bT^2$ in 2D limit, where σ_0 is residual conductivity; $alnT$ stands for both weak localization (WL) and renormalization of effective electron-electron interactions (REEI) contributions; and bT^2 is the low-temperature electron-electron Boltzmann term. All constants are positive, as shown in Table 1. The Au-LNO films show a lower T_{MIT} than the LNO films, because the weak localization in the Au-LNO films is suppressed due to the matrix LNO phase has lower concentration of oxygen vacancies. The effect of weak localization can also be reflected in the valence band changes, which will be discussed in the following part.

The valence band (VB) spectra of the LNO and Au-LNO films are shown in Fig. 5(b). Compared with the LNO film, the spectrum of the Au-LNO film shows a broad

peak, which is related to broad band of Au 5d electrons.[28] In both films, two weak peaks near Fermi level E_{Fermi} are assigned to Ni e_g and Ni t_{2g} states.[29,30] In the case of the Au-LNO films, the Ni t_{2g} peak at 1.1 eV is relatively narrow, while the Ni 3d e_g peak near the Fermi level at 0.1 eV is relatively wide, which is sensitive to oxygen stoichiometry.[29] The overlap of Ni e_g and O 2p contributes to the electron density at E_{Fermi}, which reflects the metallic nature of LNO. As mentioned above, in the Au-LNO films, Au nanoparticles can improve the crystalline quality of the LNO perovskite phase, and make it contains less oxygen vacancies. Therefore, the Au-LNO films show enhanced conductive properties due to the higher electron density at E_{Fermi} than that of the LNO films.

Conclusions

In summary, the Au-LNO nanocomposite thin films were fabricated on the Si substrates by chemical solution deposition, and their crystal structure, microstructure and electrical properties have been investigated. Au nanoparticles with average size of approximately 10 nm uniformly distribute in the composite films. The resistivity at room temperature of the Au-LNO nanocomposite thin films is about 313 μΩ·cm, which is much lower than that of the $LaNiO_3$ film (1221 μΩ·cm). The role of Au nanoparticles in the composite films can be considered from two aspects: on one hand, the uniform distribution of Au nanoparticles provides a pathway with less scattering for the conduction electrons; on the other hand, Au can serve as nuclei seeds for the crystallization of the LNO perovskite phase to improve its crystalline quality and

make it contains less oxygen vacancies. The high-quality Au-LNO nanocomposite films with a superior electrical conductivity can be used as a promising electrode for ferroelectric and multiferroic films.

Acknowledgements

The partial support of this work by the Hundred Talents Program of Chinese Academy of Sciences, and the National Natural Science of foundation of China (No. 51172238) is gratefully acknowledged.

References

1 J. Zaanen, G. A. Sawatzky, and J. W. Allen, Phys. Rev. Lett., 1985, **55**, 418.

2 D. D. Sarma, H. R. Krishnamurthy, S. Nimkar, S. Ramassesha, P. P. Mitra, and T. V. Ramakrishnam, Pramana-J. Phys., 1992, **38**, L531.

3 C. Dehoff, A. Hennings, C. Kugeler, T. Schneller, and U. Bottger, Phys. Status Solidi A, 2011, **208**, 343.

4 G. L. Smith, J. S. Pulskamp, L. M. Sanchez, D. M. Potrepka, R. M. Proie, and T. G. Ivanov, J. Am. Ceram. Soc., 2012, **95**, 1777.

5 J. F. Scott, Science, 2007, **315**, 954.

6 K. I. Park, J. H. Son, G. T. Hwang, C. K. Jeong, J. Ryu, M. Koo, I. Choi, S. H. Lee, M. Byun, Z. L. Wang, and K. J. Lee, Adv. Mater., 2014, **26**, 2514.

7 M. W. Zhu, Z. J. Wang, Y. N. Chen, H. L. Wang, and Z. D. Zhang, Appl. Phys. A: Mater. Sci. & Proc., 2012, **112**, 1011.

8 L. Qiao and X. F. Bi, Journal of Crystal Growth, 2008, **310**, 3653.

9 W. D. Wu, Y. J. He, F. Wang, Z. H. Chen, Y. J. Tang, and W. G. Sun, Journal of Crystal Growth, 2006, **289**, 408.

10 Y. J. Wu, H. L. Wang, X. K. Ning, Z. J. Wang and Q. Wang, Journal of Inorganic Materials, 2015, **30**, 207.

11 Z. R Wang., T. Hu, L. W Tang., N. Ma, C. L. Song, G. R. Han, W. J. Weng, and P. Y. Du, Appl. Phys. Lett., 2008, **93**, 222901.

12 B. Houng, Appl. Phys. Lett., 2005, **87**, 251922.

13 L. Qiao and X. F. Bi, Acta Mater., 2009, **57**, 4109.

14 T. D. Thomas and P. Weightman, Phys. Rev. B, 1986, **33**, 5406.

15 J. Zhang, Y. Gao, R. Alvarez-Puebla, J. M. Buriak, and H. Fenniri, Adv. Mater., 2006, **18**, 3233.

16 K. Tsubouchi, I. Ohkubo, H. Kumigashira, Y. Matsumoto, T. Ohnishi, and M. Lippmaa, Appl. Phys. Lett., 2008, **92**, 262109.

17 A. N. Mansour, Surface Science Spectra, 1994, **3**, 263.

18 Q. Liao, X. F. Bi, Thin Soild Films, 2010, **519**, 943.

19 M. Turner, V. B. Golovko, O. P. H. Vaughan, P. Abdulkin, A. Berenguer-Murcia, M. S. Tikhov, B. F. G. Johnson, and R. M. Lambert, Nature, 2008, **454**, 981.

20 G. Herranz, F. Sánchez, J. Fontcuberta, V. Laukhin, J. Galibert, M. V. García-Cuenca, C. Ferrater, and M. Varela, Phys. Rev. B, 2005, **72**, 014457.

21 K. P. Rajeev, A. K. Raychaudhuri, Phys. Rev. B, 1992, **46**, 1309.

22 N. D. Mathur, F. M. Grosche, S. R. Julian, I. R. Walker, D. M. Freye, R. K. W.

Haselwimmer, and G. G. Lonzarich, Nature, 1998, **394**, 39-43.

23 J. S. Zhou, L. G. Marshall, and J. B. Goodenough, Phys. Rev. B, 2014, **89**, 245138.

24 K. Yamada, T. Omata, K. Nakajima, S. Hosoya, T. Sumida, and Y. Endoh, Physica C, 1992, **191**, 15.

25 G. Q. Wu, J. J. Neumeier, and M. F. Hundley, Phys. Rev. B, 2001, **63**, 245120.

26 W. Noun, B. Berini, Y. Dumont, P. R. Dahoo, and N. Keller, J. Appl. Phys., 2007, **102**, 063709.

27 P. A. Lee and T. V. Ramakrishnan, Rev. Mod. Phys., 1985, **57**, 287.

28 M. Büttner, P. Oelhafen, Surface Science, 2006, **600**, 1170.

29 K. Horiba, R. Eguchi, M. Taguchi, A. Chainani, A. Kikkawa, Y. Senba, H. Ohashi, and S. Shin, Phys. Rev. B, 2007, **76**, 155104.

30 S. R. Barman, A. Chainani, and D. D. Sarma, Phys. Rev. B, 1994, **49**, 8475.

Figure Captions:

Fig. 1 XRD patterns of the LNO and Au-LNO thin films.

Fig. 2 XPS spectra at a binding energy range from 80 to 90 eV for the LNO and Au-LNO films.

Fig. 3 (a) A cross-sectional HAADF image for the Au-LNO film, (b) A HRTEM image for the Au-LNO film.

Fig. 4 XPS spectra of O 1*s* core level lines for (a) the LNO thin film and (b) the Au-LNO thin films.

Fig. 5 (a) Temperature dependence of resistivity of the LNO and Au-LNO thin films. Inset is an enlargement of 5-45 K range for the Au-LNO thin film. (b) Valence band spectra for the LNO and Au-LNO thin films.

Table 1 Metal-insulator transition temperature and fitting parameters for the LNO and Au-LNO thin films.

Sample	ρ_0 (μΩ•cm)	c (μΩ·cm/K$^{3/2}$)	σ_0 (10^{6}S/cm)	a (10^{6}S/cm)	b (μΩ·cm/K^2)	T_{MIT} (K)
Au-LNO	191	0.0244	5.12x10^{-3}	4.32x10^{-5}	3.3x10^{-3}	15
LNO	911	0.0672	0.95x10^{-3}	3.16x10^{-5}	0.57x10^{-3}	50

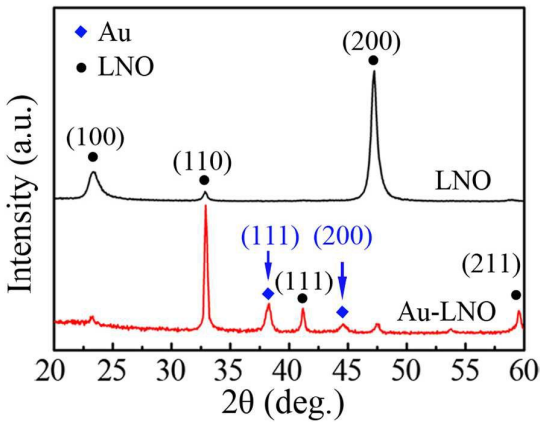

Figure 1

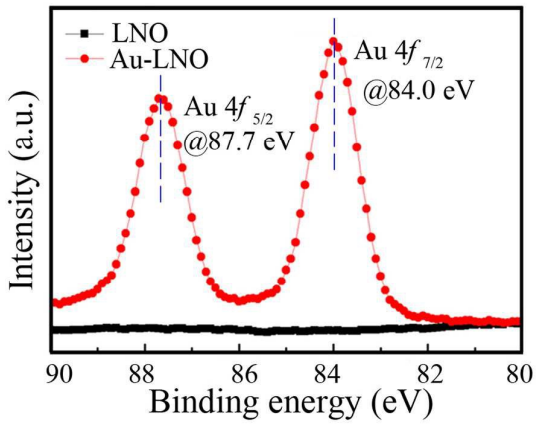

Figure 2

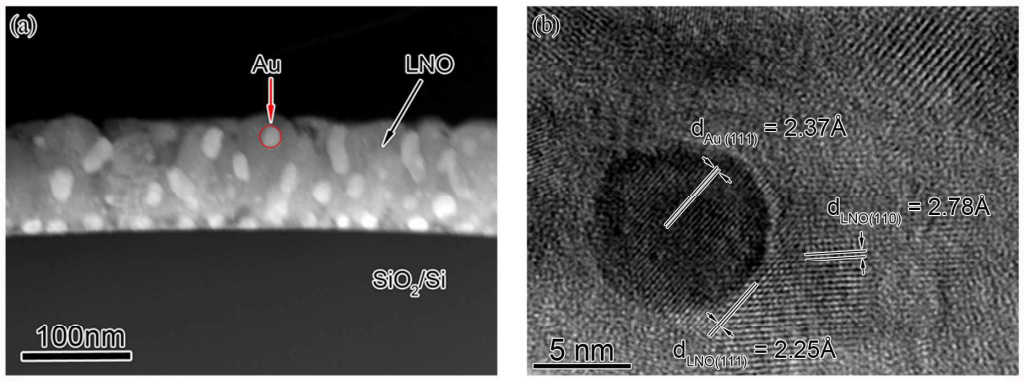

Figure 3

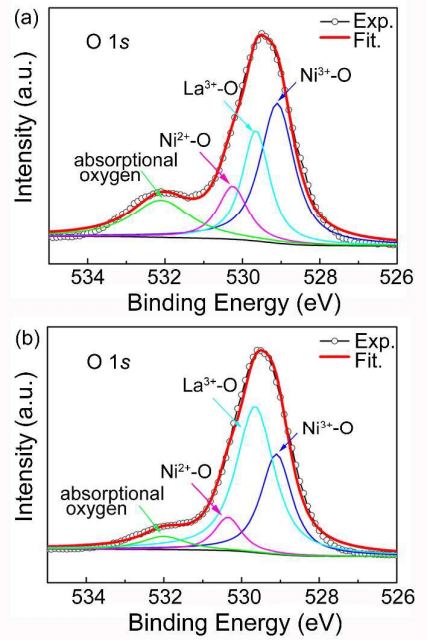

Figure 4

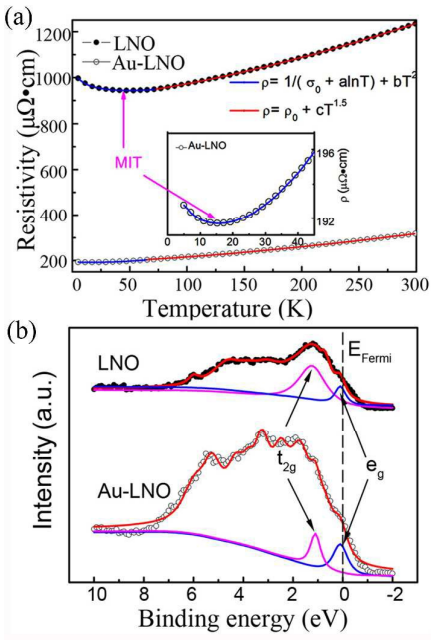

Figure 5